The role of a-axis grains in the transition to the normal state of $YBa_2Cu_3O_{7-\delta}$ films and of 2G-coated conductors when induced by high electrical current densities

P. Bernstein,[1,a)] G. Ferro,[2] C. Harnois,[1] C. Mc Loughlin,[1] J. Noudem,[1] M. R. Osorio,[2] Y. Thimont,[1] J. A. Veira,[2] D. Vidal,[2] and F. Vidal[2]
[1]*CRISMAT-ENSICAEN (UMR CNRS 6508)–Université de Caen-Basse Normandie, Boulevard du Maréchal Juin, F14050 Caen cedex, France*
[2]*LBTS, Departamento de Fisica da Materia Condensada, Universidade de Santiago de Compostela, Santiago de Compostela E15782, Spain*

The influence of surface defects, in particular of a-axis grains, on the transition to the normal state induced by high current densities in $YBa_2Cu_3O_{7-\delta}$ (YBCO) thin films and in a commercial 2G-coated conductor is investigated. For that purpose, the surface of the samples is observed by scanning electron microscopy and isothermal current-voltage curves are measured at different temperatures with pulsed currents up to the quenching value I*. The results show that the ratio of I* to the critical current is large if a-axis grains are not visible at the surface of the YBCO films, while it is much lower if the surface includes a-axis grains as this is the case for the coated conductor. The connection between the transition onset and the vortex dynamics, as well as the role of the a-axis grains in this process are discussed. The relation between the I* values obtained from thermal calculations and those resulting from vortex dynamics considerations is also discussed, as well as the possible consequences suggested by this work for the different applications of the coated conductors.
[http://dx.doi.org/10.1063/1.4864713]

I. INTRODUCTION

Applications benefiting from the capability of high T_c superconductors to carry high current intensities at the liquid nitrogen temperature begin to be available. They include cables for the transportation of large currents and also fault current limiters designed to protect electrical equipments from damages due to the large currents resulting from possible short-circuits. In resistive fault current limiters, a transport current with an amplitude larger than a threshold called supercritical current, I*, drives superconducting films inserted in the power lines to the normal state, limiting the current amplitude in the protected circuits (see as examples Refs. 1 and 2). The driving force behind these developments has been the fabrication on a more and more industrial scale of the so-called 2G coated conductors (CCs). Coated conductors consist of a c-axis oriented film of the $YBa_2Cu_3O_{7-\delta}$ (YBCO) family grown on a stack of insulating buffer layers deposited on a metallic substrate and protected by one or more metal overlayers.[3]

Understanding the processes occurring during the transition to the normal state of their superconducting film when induced by the application of large currents is of first importance for the implementation of devices including CCs in the power grids, as well as from the fundamental point of view. Current I* can be equal to but is generally larger than I_c, the critical current that defines the resistivity onset. Observations and numerical simulations of the processes occurring around I* in the CCs have shown that the transition is due to the expansion of normal zones generated at some locations in the superconducting film.[4–6] The first generated normal zones correspond to weak superconducting areas that can be due either to inhomogeneities resulting from the CCs fabrication process, for example, thickness fluctuations, or to other factors such as the strains caused by the coil winding process.[7]

The results summarized above, however, do not describe the initial processes that drive the material to the normal state. As the manufacturers improve the quality and the homogeneity of the CCs, the knowledge of these processes takes an increasing importance. According to the different models, the transition to the normal state of the films of the YBCO family can be due to either: (i) the Larkin–Ovchinnikov process, (ii) the self organized criticality of the vortex lines, (iii) the generation of phase slips centers (PSCs), (iv) the self-heating of the sample, and (v) the depinning of vortices located in the middle of the sample.

In the Larkin-Ovchinnikov model, the electric field generated by the vortex motion shifts upwards the energy distribution of the quasi-particles with respect to the equilibrium distribution.[8–10] As a consequence, the quasi-particles leave the vortex core, the viscous damping coefficient of the vortices is reduced and the vortex velocity increases, until an instability point is reached. However, some authors have claimed that this model does not account for all the features of the transition in the films of the YBCO family.[11]

The model of the self organized criticality of the vortex rows suggests that the discontinuity at the transition is due to the jump of a vortex line that triggers a chain reaction in the vortex rows or an avalanche.[12] This model is supported by computer simulations,[13] magneto-optical observations,[14] and theoretical calculations.[15] Nevertheless, different physical phenomena can cause the initial flux jump.

[a)]E-mail: pierre.bernstein@ensicaen.fr

In principle, phase slips centers occur in 1D systems only, however, several groups have claimed that they have observed PSCs in films.[16–18] At a PSC location, the modulus of the order parameter vanishes periodically with the Josephson frequency while the phase changes by 2π. Then, the area of the PSC turns resistive and the voltage experiences a discontinuity. As a result, the current-voltage curves show several small voltage jumps, each corresponding to the ignition of a determined PSC, before the transition to the normal state occurs. Many measurements, however, report no discontinuity in the current-voltage curves before the transition.[19–21]

Models based on the self-heating of the samples have resulted in a good reproduction of the experimental results obtained on films[6,20–24] as well as on coated conductors.[25] They permit one to determine I* from both the thermal impedance of the substrate and the current-voltage characteristics of the film but they do not consider the physical phenomena determining the shape of the characteristics.

The model based on the depinning of vortices located in the middle of the sample supposes that in absence of an external magnetic field, vortices and anti-vortices enter opposite edges of the superconducting film and annihilate each other along an annihilation line. It suggests that for a large enough transport current the constructive interference of the screening currents due to the vortices and anti-vortices located in the vicinity of the annihilation line causes the depinning of the vortices located in this area, starting an avalanche.[26] Strangely, both this last model and the thermal model have provided neighbouring I* values for the same samples, although their physical grounds are very different. However, the model based on vortex depinning has proved ineffective in the case of some other samples.

In this contribution, we compare pulsed current measurements and scanning electron microscopy (SEM) observations carried out on YBCO films fabricated according to different techniques to similar measurements and observations carried out on a commercial coated conductor. The microscopic observations show striking differences in the surface aspect of the various samples that are related to their electrical properties. Namely, the electrical characteristics and the surface aspect of the coated conductor are similar to those of the films whose transition cannot be described by the depinning of the vortices located in the middle of the sample. After reviewing the main aspects of this model, another description of the vortex dynamics at the transition, relevant for both these films and the CC and consistent with the SEM observations and the electrical measurements is proposed.

In Sec. II, we present the samples and the pulsed current measurements systems used to determine their current-voltage characteristics. The results of the measurements and SEM observations are reported in Sec. III. The models we propose to reproduce them are presented in Sec. IV. Section V is devoted first to a discussion of the puzzling observation that the transition to the normal state can be described with both the thermal models and the models based on vortex dynamics. Then, some possibilities for the improvement of the properties of the 2G-coated conductors resulting from this work are detailed.

II. SAMPLES CHARACTERISTICS AND MEASUREMENTS TECHNIQUES

A. Samples

The measurements and SEM observations were carried out on three YBCO bridges deposited on $SrTiO_3$ substrates and on a commercial coated conductor (SF4050AP) fabricated by SuperPower Inc. (www.superpower-inc.com). Films M222E and M225A were fabricated by sputtering and patterned as microbridges by UV photolithography and wet chemical etching. Film HoL01 was grown by pulsed laser ablation and patterned by Ar ion milling. Complete details about the fabrication and the general characteristics of the samples have already been published for both sputtered[20,27] and laser ablated[21,28] films. The dimensions and critical temperature of the micro-bridges investigated are reported in Table I. The coated conductor consists of a $YBa_2Cu_3O_7$ film whose thickness is in the micrometer range grown on a stack of buffer layers deposited on a 4 mm wide Hastelloy strip and covered with an Ag overlayer. Its critical temperature, T_c, is equal to 88.7 K. It includes nano-particles for reinforcing vortex pinning and was specially designed for fault current limiters.

B. Measurement of the current-voltage curves with current pulses

For both the microbridges and the CC, the current-voltage curves were measured by applying current pulses in the millisecond range. For the micro-bridges we have used a Keythley 2425 current source and for the CC a LAB/SM835/4001/ATI-10 from ET system electronic GmbH. During the current pulses, the voltage at the samples terminals was measured with National Instruments high-speed data acquisition cards (PCI-5122 for the micro-bridges and PCI-4452 for the CC). In the case of the micro-bridges, the measurements were carried out while the samples were held in a He gas atmosphere,[20] whereas the CC was immersed in pressurized liquid nitrogen.[19,27] As a consequence, while measurements on the micro-bridges could be carried out above and below the liquid nitrogen temperature, measurements on the coated conductor could be achieved above 77 K only. Additional measurements, that will be described in details in a forthcoming paper, were carried out with 4 μs pulses on bridge HoL01 and are also reported.

III. RESULTS

In this section, the current-voltage measurements carried out with pulses in the millisecond range on the coated

TABLE I. Length L, width w, thickness d, and critical temperature T_c of the micro-bridges investigated in this work. The micro-bridges have the same name as the films from which they were patterned.

Bridge	L (μm)	w (μm)	d (nm)	T_c (K)
M222E	800	80	100	90,7
M225A	800	60	100	89,5
HoL01	500	50	150	87.2

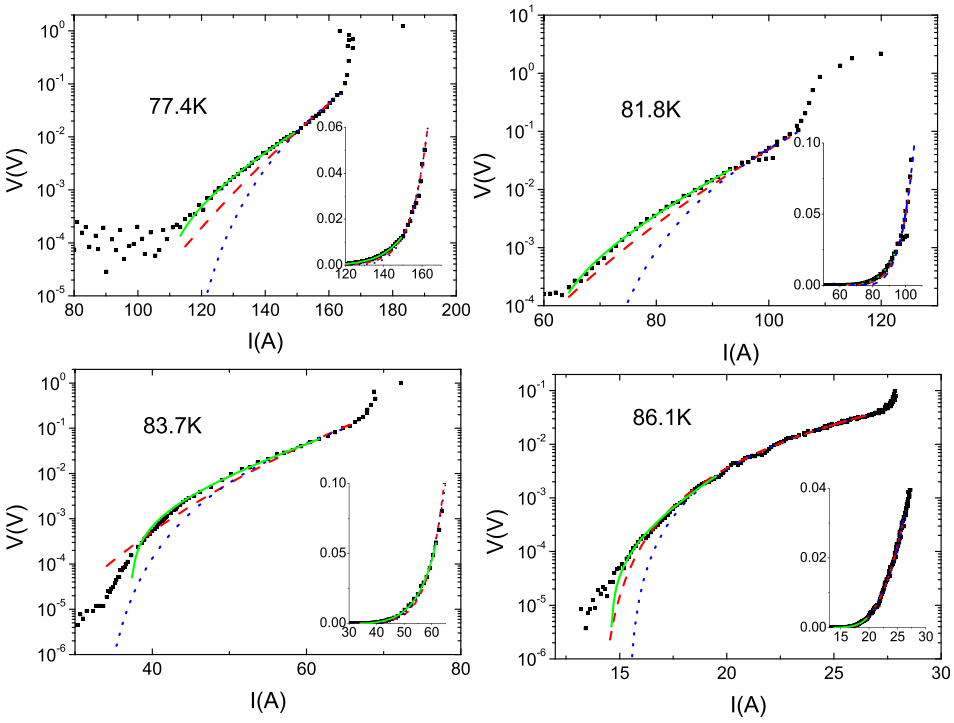

FIG. 1. Current-voltage characteristics of the coated conductor SF4050AP at various temperatures above 77 K. The black dots are the experimental measurements. The red dash lines are the best fits to data obtained with the power law of the Zeldov model. The blue dot lines are the best fits obtained with the critical power law. The green solid lines are the best fits obtained with Eq. (9). The insets show the same curves on a linear scale.

conductor and on the bridges are confronted with the surface images obtained by SEM.

Figures 1(a)–1(d) show the current-voltage curves measured at various temperatures on the SF4050AP coated conductor and Figs. 2(a)–2(c) those measured on the microbridges at 77 K.

All the I-V curves are typical of the flux creep regime below the transition and, as in Refs. 19 and 21, they show no discontinuities, suggesting that the PSCs play no role in the transition to the normal state of the investigated samples. The current-voltage curves of the coated conductor are strikingly different from those obtained with current pulses in the 15 μs range.[29,30] These curves were typical of the flux creep regime just above I_c only and included two linear sections with different slopes before the transition to the normal state. The reasons for these differences are not clear and should be investigated in the future. Figure 3 shows the ratio $\frac{I*}{I_c}$ for the coated conductor and the investigated bridges. This quantity is clearly larger for bridge HoL01 than for the other samples that show very similar values. The difference is not linked to the technique used for the fabrication of the samples, since the films investigated in Ref. 26 were prepared by sputtering, as were films M222A and M225E, while their $\frac{I*}{I_c}$ ratio was in the same range as that of bridge HoL01. Figure 4 shows SEM pictures of the surface of bridges M222E and M225A. They present defects aligned along two perpendicular directions in a c-axis textured matrix. The length of most of these defects lies between 0.5 and 2 μm.

While some defects look crystalline, others consist of small crystallites aligned along the same two perpendicular directions as the defects themselves. This can be seen in the inset that shows a high magnification picture of a defect of film M222E.

The metal overlayer of the SF4050AP coated conductor was stripped off with a solution containing H_2O_2 (25%), NH_4OH (25%), and H_2O (50%) revealing the superconducting film. The surface of this film, shown in Fig. 5, includes many defects with no special shape, that according to energy dispersive X-Rays spectroscopy are probably CuO grains. The film includes also defects with a length in the same range as in films M222E and M225A and aligned along two perpendicular directions.

The high magnification picture in the inset of Fig. 5(a) shows that these defects are crystalline. While many of them are scattered with a surface density much lower than in the microbridges, they can also build structures at some places, as seen in Fig. 5(b). The presence of a-axis grains in coated conductors with a size and a shape similar to the defects in Fig. 5 has been previously reported,[31,32] suggesting that the crystallites observed in the SF4050AP and in films M222E and M225A are also a-axis grains. Figure 6 shows the surface of film HoL01. Film HoL01 includes no a-axis grains.

As a conclusion for this section, the results suggest that a low $\frac{I*}{I_c}$ ratio is linked to the presence in the superconducting films of a-axis grains or of domains including a-axis grains, while a higher ratio is obtained if they are absent.

IV. MODELS

As a general rule, the power dissipated in YBCO films above the critical current is attributed to the motion of vortices previously pinned in the bulk of the films. The most popular model accounting for the vortex dynamics is the Zeldov model.[33] It predicts a $V \propto I^n$ relationship, where n is an exponent depending as $n = \frac{U}{k_B T}$ on the vortex pinning energy U and the temperature. For all the samples, at all the investigated temperatures, there is always a n-value fitting the high voltage part of the I-V curves. The low voltage part of the I-V curves, however, is often badly reproduced, as seen in Figs. 1 and 2. Plotting the n values as a function of the

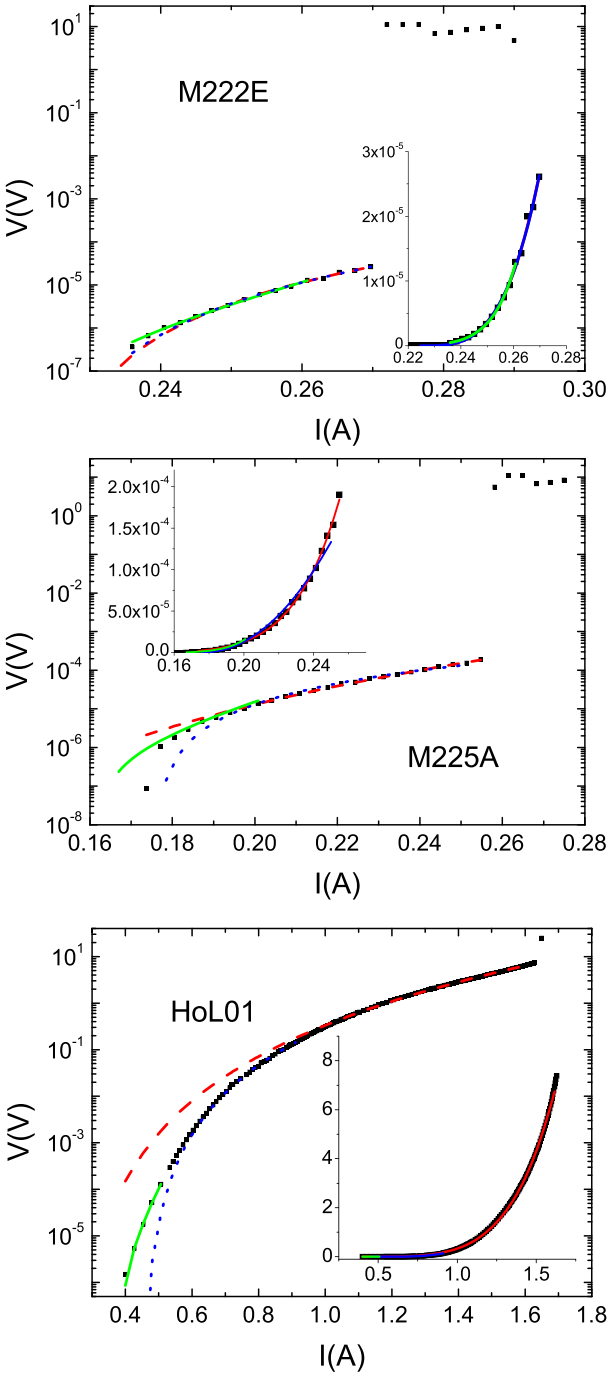

FIG. 2. Current-voltage characteristics of films M222A, M225E, and HoL01 at 77 K. The black dots are the experimental measurements. The red dash lines are the best fits to data obtained with the power law of the Zeldov model. The blue dot lines are the best fits obtained with the critical power law. The green solid lines are the best fits obtained with Eq. (9). The insets show the same curves on a linear scale.

reduced temperature T/T_c (see Fig. 7(a)) shows that the error on the value of n can be large, as it is the case for the CC and the M222E micro-bridge near T_c. In addition, no features common to some samples that could correspond to the observations made in Sec. III are visible. The main problem with the Zeldov model, however, is that it is not consistent with the critical state model,[34,35] whose validity for YBCO has been verified experimentally.[36,37] As a result, other power laws taking into account the existence of the critical current

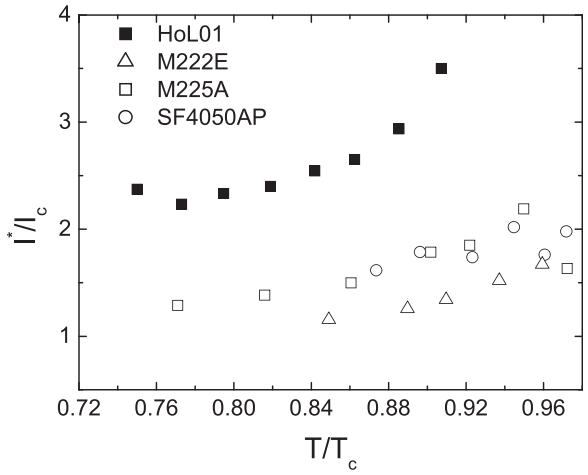

FIG. 3. Ratio $\frac{I_c^*}{I_c}$ of the supercritical to the critical current for the investigated samples as a function of the reduced temperature $\frac{T}{T_c}$.

have been proposed. For example, Viña *et al.*[20] have proposed what they have called the Critical Power Law (CPL) that takes the form

$$V = V_c\left(\frac{I}{I_c} - 1\right)^n, \tag{1}$$

where V_c is a fitting parameter. Equation (1) permits one to reproduce the high voltage part of the I-V curves as well as the Zeldov model (see Figs. 1 and 2) with n values that are different from those given by this last model, as seen in Fig. 7(b). However, the calculated voltages generally show also large discrepancies with the measurements in the low voltage region. While the error when determining n is smaller with the CPL than with the Zeldov model, as it was the case for this model, no feature in the $n(T/T_c)$ curves accounting for the behaviour of the samples is visible.

In previous articles,[38,39] some of us have suggested that the shape of the I-V curves at low current above I_c is due to the motion of vortices located in the twin boundaries (TBs) of YBCO films. They have also suggested that the sudden change in the power dissipated by the sample, leading to its transition to the normal state, can be due in some cases to the depinning of these vortices.[26] In this section, we remind in a slightly modified form of the main aspects of the models proposed in Refs. 26, 38, and 39 to describe the vortex dynamics of YBCO films in the critical state or at low current above I_c and their transition to the normal state. We show that they yield a good reproduction of the I* of film HoL01, as they did with the films examined in Ref. 26, but neither of the I* of films M222E and M225A nor of those of the SF4050AP coated conductor. Then, we describe how the presence of a-axis grains can play a role in the transition to the normal state of these last samples.

A. Vortex dynamics at low current above the critical value

In Refs. 26, 38, and 39, we have considered the flux creep regime in the critical state or just above I_c in a YBCO bridge or strip with no applied magnetic field. According to the

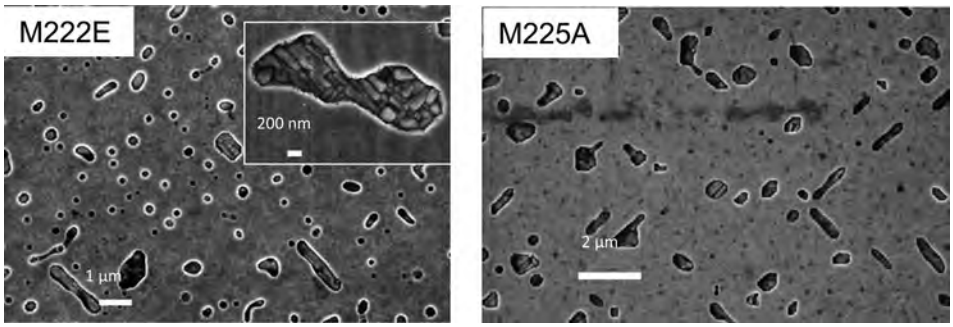

FIG. 4. Scanning electron micrograph of bridges M222E and M225A. The inset in the micrograph of bridge M222E shows a high magnification picture of a surface defect.

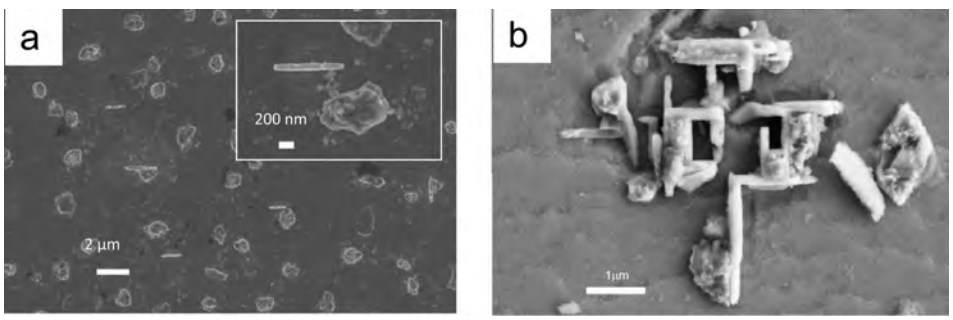

FIG. 5. Scanning electron micrographs of the YBCO film included in the coated conductor. The inset in Fig. 5(a) shows a high magnification picture of an a-axis grain.

critical state model, as the current increases from zero, vortices and anti-vortices enter the peripheral part of the superconducting film, while the central area remains flux and current free for $I < I_c$.[36,40] The area of the current and flux free central region decreases as the current increases and the vortices and anti-vortices are set in motion when it disappears. The film is then in the critical state ($I = I_c$). It was shown, however, that vortex bending can permit the motion of the vortices for currents lower than that corresponding to the destruction of the flux free region.[41] This phenomenon has hampered the fabrication of CCs with a large thickness and a large critical current for some time and was overcome only by the introduction in the superconducting films of nano-particles modifying vortex bending.[42] The vortex dynamics described here does not take this phenomenon into account.

Following magneto-optical observations, the TBs are the first areas occupied by the vortices in YBCO.[43] We have considered that at low current the flux creep regime corresponds to the motion of the vortices located in the TBs, while most of the vortices in the bulk of the films are pinned. In this description, the TBs act as grooves channeling the vortices and the anti-vortices, since pinning is strong in the direction perpendicular to the TBs direction and weak along the TBs. For $I \geq I_c$, vortices and anti-vortices are supposed to move along the TBs in opposite directions and to annihilate each other in the middle of the sample along an annihilation line. Otherwise, since the TBs width in YBCO is in the range of $\xi_{ab}(T)$, the superconducting coherence length in the a-b planes, some type of Josephson behaviour can be expected.[44–47] However, the TBs in YBCO are highly disordered.[48,49] This is the reason why we have suggested that they split into superimposed rows de Josephson weak links (JWLs). The coupling energy of the JWLs must be at least equal to $k_B T$, in order to maintain the phase coherence of the order parameter across the TBs. The corresponding current amplitude is[50]

$$I_J = \frac{2\pi k_B T}{\phi_o}, \tag{2}$$

where ϕ_0 is the flux quantum. In the critical state, all the weak links are expected to carry current I_J (except those at the vortex cores). As a result, if the superconducting film includes Z rows of JWLs that all carry current, its sheet critical current density takes the form

$$J_c \approx Z\frac{I_J}{\bar{\delta}}, \tag{3}$$

where $\bar{\delta}$ is the mean length of the JWLs along the TBs. As shown in Ref. 38, $\bar{\delta}$ decreases strongly as the temperature decreases. As a result, the J_c values calculated with Eq. (3) are increasing as the temperature decreases, as observed experimentally. Since the vortex cores go across the film, they are carried by Z superimposed weak links in the TBs and it is reasonable to assume that the vortex motion is due

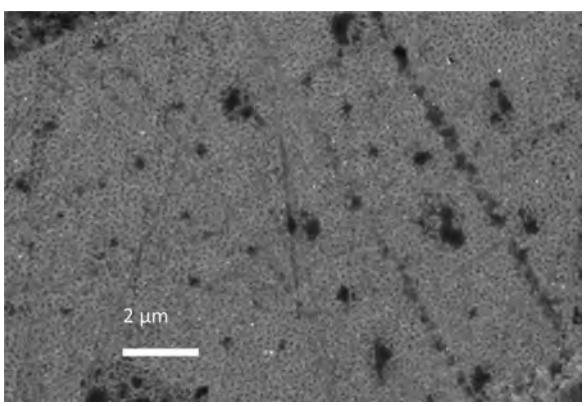

FIG. 6. Scanning electron micrograph of bridge HoL01.

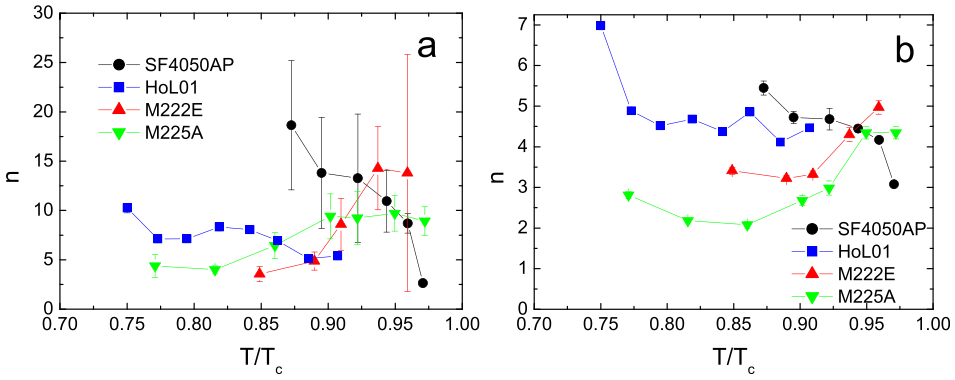

FIG. 7. n values obtained by fitting the Zeldov power law (Fig. 7(a)) and the critical power law (Fig. 7(b)) to the current-voltage curves of the investigated samples.

to the successive displacement of the core sections carried by the different rows, from a JWL to the next one in the same row. The corresponding average displacement for the whole vortex is equal to $\frac{\bar{\delta}}{Z}$. According to Ref. 51, pinning in the TBs is due to the repulsive interaction of two vortices located on intersecting TBs. Then, the distance between two sections of the cores of these vortices decreases only if a screening current line due to each of them enters the core of the other one with amplitude I_J. The corresponding energy barrier or pinning energy takes the form

$$U_o = 2I_J\Phi, \tag{4}$$

where Φ is the magnetic flux carried by a vortex. In a classical description, the vortices carry one flux quantum in order to maximize the superconducting-normal interfaces. The results reported later in the paper suggest, however, that Φ for bridge HoL01 is equal to two flux quanta, as reported for some of the films investigated in Refs. 26 and 38. This possibility is supported by scanning SQUID microscopy of the flux generated by vortices pinned in a strip that has also suggested the existence of vortices carrying several flux quanta.[52] Another possibility is that the screening current lines do not sweep single vortices but flux bundles. Flux creep results from thermal activation. In the framework of the Kim-Anderson model[53] and consistently with the critical state model, the current-voltage relation of a bridge with width w in the flux creep regime can be written as

$$\frac{V}{w} = r_a(J - J_c)e^{-\frac{U_0}{k_BT}}\sinh\left[\frac{W}{k_BT}\right]. \tag{5}$$

In Eq. (5), r_a is related to the bridge and J and J_c are, respectively, the transport and the critical sheet current densities. W is the work carried out by the current during a vortex line displacement on distance $\frac{\bar{\delta}}{Z}$. We have

$$\frac{W}{k_BT} = \frac{J\Phi}{k_BT}\frac{\bar{\delta}}{Z} = \frac{J}{J_\delta} \tag{6}$$

with

$$J_\delta = \frac{Zk_BT}{\Phi\bar{\delta}}. \tag{7}$$

From Eqs. (2), (3), and (7), we obtain the relation

$$J_c = 2\pi\frac{\Phi}{\phi_0}J_\delta, \tag{8}$$

connecting the critical sheet current density to J_δ. This last quantity is related to the I-V curvature and can be obtained by fitting the low current part of these curves with the expression

$$\frac{V}{w} = R_a(J - J_c)\sinh\left[\frac{J}{J_\delta}\right], \tag{9}$$

where R_a is a fitting parameter. In Figs. 1 and 2, we have reported the fitting curves obtained with Eq. (9). At low current, they are clearly in a better agreement with the measurements than those obtained with the Zeldov power law and the CPL. Equation (8) or equivalent relations involving the critical current or the critical current density have been verified on many samples in a large range of temperatures.[26,38] As examples, the experimental J_c of films HoL01, M222E, M225A and of the coated conductor are compared to the values calculated with Eq. (8) in Figs. 8 and 9, taking $\Phi = \phi_0$ for all the samples, except film HoL01 and $\Phi = 2\phi_0$ for film HoL01. Here, we have supposed that the current flows only in the superconducting film of the SF4050AP coated conductor. For all the samples, the calculated J_c are in the range of the measured values, although the errors are larger for bridge

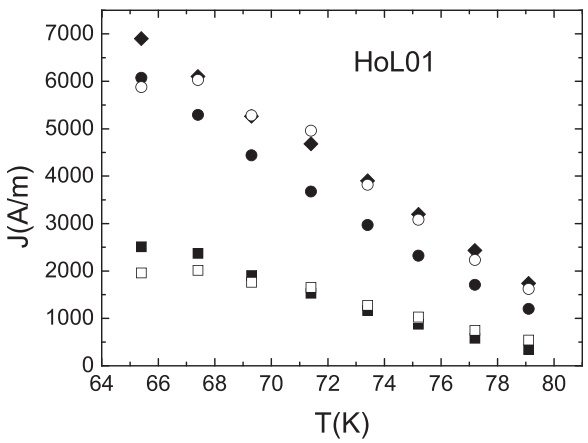

FIG. 8. Comparison of the calculated critical and supercritical sheet current densities to the measurements carried out on bridge HoL01; (■): measured critical sheet current densities. (□): sheet current densities calculated with Eq. (8); (●): supercritical sheet current densities measured with 800 μs pulses; (◆): supercritical sheet current densities measured with 4 μs pulses; (○): supercritical sheet current densities calculated with Eq. (13).

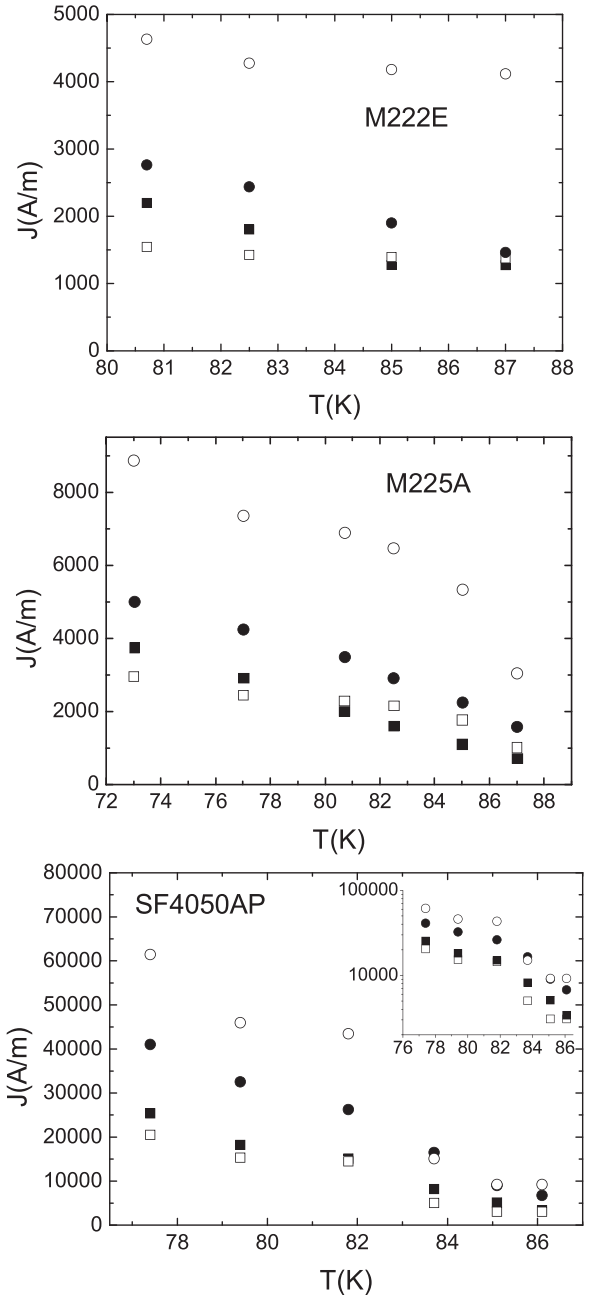

FIG. 9. Comparison of the calculated critical and supercritical sheet current densities to the measurements carried out on bridges M222E and M225A and on coated conductor SF4050AP. (■): measured critical sheet current densities; (□): sheet current densities calculated with Eq. (8); (●): measured supercritical sheet current densities; (○): supercritical sheet current densities calculated with Eq. (13). The inset shows a semi-log plot of the same quantities for CC SF4050AP.

M222E than for the other samples. The reason for this lack of accuracy is the low number of measurements in the vicinity of J_c carried out on this sample.

We stress again that the domain of validity of Eqs. (5) and (9) is limited to the low current part of the current-voltage curves. The reason for this restriction is that we have supposed that only the vortices located on the TBs are in motion at low current, while it is probable that more and more vortices located in the bulk of the films take part to the flux creep as the current increases, yielding a power law for the current-voltage relation.

B. Transition to the normal state

In the framework of vortex dynamics, the transition to the normal state is linked to the massive depinning of vortex lines. Depinning of an individual vortex line occurs if the total force $\vec{F}$ acting on the vortex is equal to the maximum value of the pinning energy gradient.

Since the pinning energy is an elastic energy,[54,55] the maximum amplitude of the force acting on a vortex located in a TB can be written as

$$F = J_{\text{core}}\Phi = 2Z\frac{U_o}{\bar{\delta}}, \tag{10}$$

where J_{core} is the sheet current density in the vortex core.

From Eqs. (3), (4), and (10), we obtain

$$J_{\text{core}} = 4Z\frac{I_J}{\bar{\delta}} = 4J_c. \tag{11}$$

Equation (11) means that the depinning of a vortex line occurs when the current carried by each JWL of its core is equal to $4I_J$. To account for the values of J*, we have considered that if a current with sheet density $J \geq J_c$ flows in a film, the inter-vortex distance along a TB in the vicinity of the annihilation line is

$$d_{vv} = 2\lambda_{ab}\frac{J_c}{J}, \tag{12}$$

where λ_{ab} is the superconducting penetration depth in the a-b planes of YBCO. Equation (12) yields the reasonable result that, in the critical state, $d_{vv} = 2\lambda_{ab}$ in the middle of the film. Therefore, we assume that the screening current of a vortex is equal to I_J across the JWLs located at a distance less than λ_{ab} from its core and is equal to zero across the other JWLs. For $J = 3J_c$, the sum of the screening currents due to their first and second neighbouring vortices and anti-vortices flowing across the weak links located on the annihilation line is equal to $4I_J$ (see Fig. 10). As a result, J* is written as

$$J* = 6\pi\frac{\Phi}{\phi_0}J_\delta, \tag{13}$$

because, as the current goes on increasing, more weak links in the cores of the vortices neighbouring the annihilation line carry current $4I_J$ and we can expect a thermal runaway due to the vortices located in the TBs for a current density very near the value given by Eq. (13). For the calculations, Eq. (13) is preferred to the simpler relation $J* = 3J_c$, because, for reasons briefly described at the end of this section and detailed in Ref. 26, the discrepancies between the measured and the calculated J_c can be important in the vicinity of T_c. The J* measured with 800 μs and 4 μs pulses on bridge HoL01 are compared to the values calculated with Eq. (13) in Fig. 8. The calculated J* are above the measurements carried out with the long pulses but fall almost exactly on those carried out with the 4 μs pulses. Fig. 9 shows the experimental and calculated J* for bridges M222A, M225E and for the coated conductor.

The calculated J* are much larger than the experimental ones for bridges M222E and M225A. For $T < 83$ K, the J* calculated for the coated conductor are different from the measured values but look correct at higher temperatures. However,

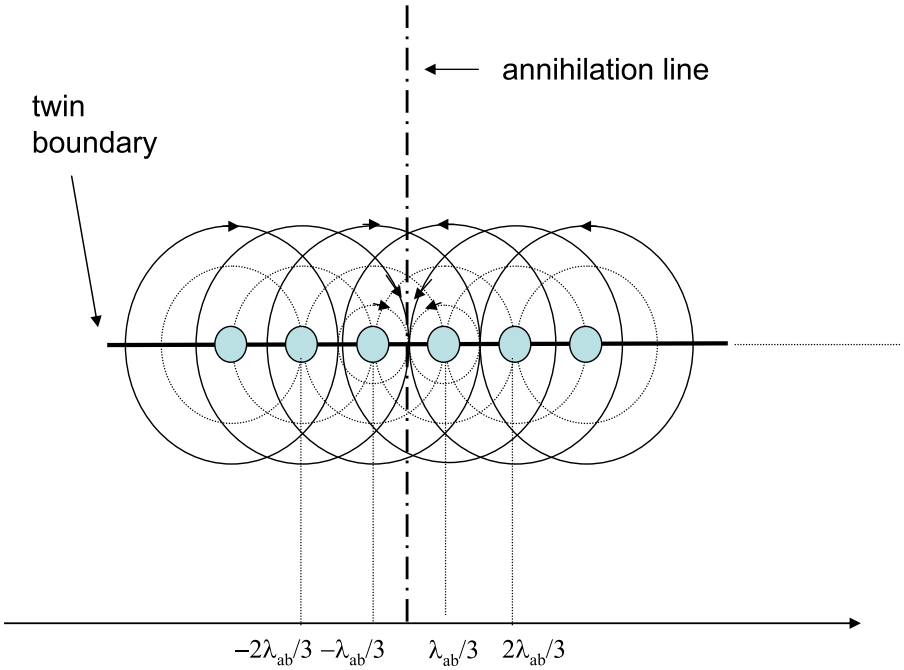

FIG. 10. Schematic representation of the vortices and anti-vortices lying along a twin boundary in the vicinity of the annihilation line for $J = 3J_c$. For the sake of clarity, the screening current lines are shown as circles and the grey areas in the circles represent the vortex cores. The thick and the vertical dash lines represent the twin boundary and the annihilation line, respectively. The amplitude of the screening current of a vortex across a JWL is equal to I_J if the distance to its core is lower than λ_{ab} and equal to zero in the opposite case. The sum of the screening currents due to their first and second neighbours across the JWLs located along the annihilation line current is equal to $4I_J$.

the semi-log plot in the inset of Fig. 9 shows that the calculated critical sheet current densities are under-estimated at 83.5 K and 85.1 K. This suggests that J_δ and, as a result, the calculated J* are under-estimated at these temperatures and that there is in fact no agreement between the measured and the calculated J*. Clearly, the transition to the normal state of bridges M222E, M225A and of the coated conductor does not result from the depinning of the vortices in the TBs neighbouring the annihilation line. We suggest instead that it is due to the depinning of the vortices located in their a-axis grains. The a-axis grains do not include TBs, except at the location of the possible connections to perpendicular ones. We suggest that there is no individual pinning of the vortices located in the a-axis grains and that pinning is effective for preventing the vortices from exiting the grains only. As a result, each vortex in a grain exerts a force on its next neighbour and the total force acting on the exiting vortex is the sum of the Lorentz forces acting on all the vortices in the grain. If the pinning energy keeps the form of Eq. (4), for example, if it is due to the repulsive force of vortices located at TBs intersections in the c-axis matrix at the ends of the grains, depinning will occur if the grain contains four vortices. A thermal runaway generating a normal zone dissipating enough energy to expand to the whole sample will take place if the sample includes locally a significant number of grains with more or less the same length and large enough to accommodate four vortices. From Eq. (12), the required grain length is

$$d_g = 4d_{vv} = 8\lambda_{ab}\frac{J_c}{J*}. \tag{14}$$

For YBCO the penetration depth in Eq. (14) takes the form[56]

$$\lambda_{ab}(T) = \frac{\lambda_{ab}(0)}{1 - \left(\frac{T}{T_c}\right)^2\Big)^{\frac{1}{2}}}. \tag{15}$$

Figure 11 shows the d_g values calculated with Eq. (14) and the J_c and J* values measured on the coated conductor and on bridges M222E and M225A, taking $\lambda_{ab}(0) = 145$ nm. For the coated conductor and bridge M225A, we have $d_g \approx 1.5\ \mu m$for $T/T_c \leq 0.92$. For bridge M222E, the calculated d_g lies between 1.9 μm and 2.2 μm for $T/T_c \leq 0.94$. These d_g values are in the range of the length of the a-axis grains in Figs. 4 and 5. While the large concentration of a-axis grains in films M222E and M225A suggests that the power dissipated by the depinning of the vortices they contain can be sufficient to trigger a thermal runaway, this is less evident in the case of the coated conductor, because its concentration in a-axis grains is much lower. It was shown in Ref. 57 that the internal magnetic field along the edges of a coated conductor is in the range of the irreversibility field for $I \approx I_c$. Then, for $I > I_c$, the vortices along the CC edges are probably no longer pinned. However, since in the centre

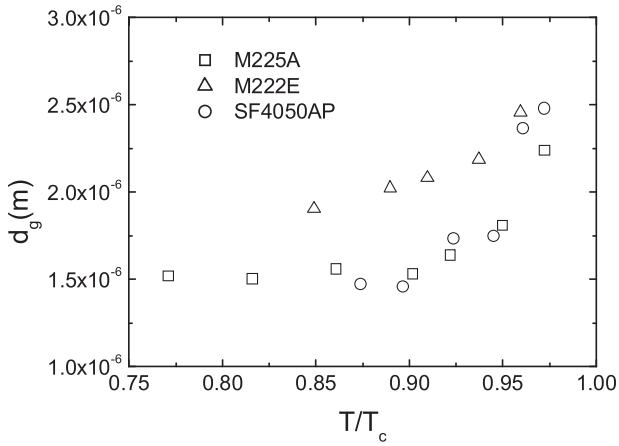

FIG. 11. Length d_g of the a-axis grains supposed to be responsible for the transition to the normal state of bridges M225A, M222E and of coated conductor SF4050AP, calculated with Eq. (14) and the $\frac{I*}{I_c}$ ratio reported in Fig. 3.

vortex motion occurs by flux creep because vortex pinning is still effective, they cannot run freely across the sample.

It is then reasonable to suppose that the thermal runaway is ignited by the combination of the release of power due to the depinning of the vortices located in the a-axis grains with the pressure exerted by the free vortices located along the edges. The proposed process can take place only if an appreciable number of a-axis grains fulfil the condition $d_g \geq \frac{8}{3}\lambda$, i.e., are long enough to accommodate 4 vortices for $J < 6\pi\frac{\Phi}{\phi_0}J_\delta$.

As a last observation, the considerations detailed above are consistent with the behavior of $\frac{I*}{I_c}$ in Fig. 3. This ratio for bridge HoL01 increases strongly near T_c. The same behavior was observed in Ref. 26. It was attributed to the presence of JWLs whose critical current is lower than I_J in this domain of temperature. These weak links give no contribution to the superconducting current flowing across the TBs. Therefore, the sample critical current is smaller than the value expected from Eq. (8). To the contrary, for $I > I_c$, the transport current flows across all the weak links because there is a voltage drop between the two banks of the TBs. This results in I* values that are near those calculated with Eq. (13) in the whole temperature range and $\frac{I*}{I_c}$ ratios that increase as T increases in the vicinity of T_c. In the case of bridges M222E and M225A and of CC SF4050AP, as for bridge HoL01, a reduction in I_c is expected near T_c in addition to that due to the temperature increase. This results in a lower $\frac{I*}{I_c}$ increase than in bridge HoL01 because I* is also reduced with respect to the values expected. The reason is that the release of power required for the transition to the normal state is smaller near T_c than at lower temperatures. Otherwise, the a-axis grains population includes an appreciable number of grains with a length larger than that obtained with Eq. (14). The density of these grains is not large enough for the depinning of their vortices to release enough power to trigger a thermal runaway, except in the vicinity of T_c. As a consequence, I* is reduced in this region and partially offsets the decrease of I_c.

V. DISCUSSION AND CONCLUSION

In this section, we discuss first the reasons why the thermal models and the models proposed in Sec. IV yield similar values for I*. Then, we address the possible consequences of this work on the design and the fabrication of the 2G-coated conductors.

Let us consider the samples whose surface includes no a-axis grains or only a-axis grains so small that they do not fulfil the conditions mentioned at the end of Sec. IV. For $I \gg I_c$, the thermal dissipation arises mainly from the motion of vortices located in the bulk of the superconducting film. Then, using a power law for the current-voltage relation, the thermal models can determine the supercritical current as a function of both the power dissipated during the application of the current pulses and the thermal properties of the substrate, as done in Refs. 20, 21, 24, and 25. The results reported in Fig. 8 suggest, however, that the upper limit of the supercritical current measured when reducing the pulses duration is the value calculated with Eq. (13). The probable reason is that a large increase in the dissipated power rate triggers a thermal runaway[20] and it is reasonable to assume that this occurs necessarily when the vortices located in the TBs are suddenly set free. Otherwise, the upper limit of J* can be approached only if the thermal energy released by the vortex motion is not sufficient for triggering the transition to the normal state, i.e., if the pulse duration is short. This proposition is supported by the results reported by various authors who have measured $\frac{I*}{I_c} \approx 3$, as predicted by the model described in Sec. IV.[19,58,59]

We discuss now the transition of the samples including a-axis grains. As mentioned at the end of Sec. IV, they include an appreciable number of grains with a length larger than the d_g values calculated with Eq. (14). The depinning of the vortices located in these grains does not trigger a thermal runaway (except in the vicinity of T_c, as seen in Sec. IV) but it results in an increase of the voltage generated in the bridge. This voltage increase adds up to that due to the motion of the vortices located in the bulk of the films, as soon as the vortices in the longest grains are depinned, modifying the shape of the I-V curves. The current density for which the power dissipated is so large and increases so strongly that it cannot be evacuated by the substrate can then be predicted with thermal models, taking the modified I-V curves into account.

The factors influencing the expansion velocity of the normal zones during the transition to the normal state in CCs have been thoroughly investigated. The role of the thermal properties of the substrate as well as that of the thickness of the metal overlayer have been examined.[6,60,61] With respect to these results, the main conclusion of our work is that we cannot discard the possibility that the existence of a-axis grains in the superconducting films included in CCs has also a strong influence on the transition. In this case, the data reported in Fig. 11 suggest that the maximum value of the supercritical current could be determined when fabricating the coated conductor if the length of the a-axis grains was controlled. Otherwise, if the superconducting films were free of a-axis grains (or included very small grains only), one can suppose that fault currents with a limited amplitude would not cause necessarily the quenching of the CCs, since the $\frac{I*}{I_c}$ ratio are larger in this situation than if a-axis grains are present. This would be an advantage in most applications other than the limitation of fault currents. Previous works on YBCO films deposited on various substrates have shown that the growth of the a-axis instead of the c-axis phase depends on the preparation conditions of the films, especially the growth temperature.[62–64] It is reasonable to suppose that the length of the a-axis grains or their absence in the YBCO films could be controlled by the introduction of suitable parameters at some steps of the fabrication of the coated conductors.

ACKNOWLEDGMENTS

The contributions of the LBTS have been supported by Spain's Ministerio de Ciencia e Innovacion Project No. FIS2010-19807, by the Xunta de Galicia 2010/XA043 and 10TMT206012PR projects, and by the European project ENERMAT. All these projects are co-funded by ERDF from the European Union.

[1]C. A. Baldan, J. S. Lamas, C. Y. Shigue, and E. R. Filho, IEEE Trans. Appl. Supercond. **19**, 1810 (2009).
[2]S. Kara, S. Kulkarni, M. Dixit, K. Pal Singh, A. Gupta, P. V. Balasubramanyam, S. K. Sarangi, and V. V. Rao, Phys. Proc. **36**, 1231 (2012).
[3]H. Kumakura, Jpn. J. Appl. Phys. **51**, 010003 (2012).
[4]S. Torii, S. Akita, Y. Iijima, K. Takeda, and T. Saitoh, IEEE Trans. Appl. Supercond. **11**, 1844 (2001).
[5]A. Ishiyama, M. Tsuchiya, H. Ueda, and Y. Shiohara, IEEE Trans. Appl. Supercond. **17**, 3765 (2007).
[6]F. Roy, M. Therasse, B. Dutoit, F. Sirois, L. Antognazza, and M. Decroux, IEEE Trans. Appl. Supercond. **19**, 2496 (2009).
[7]A. L. Mbaruku, U. P. Trociewitz, X. Wang, and J. Schwartz, IEEE Trans. Appl. Supercond. **17**, 3044 (2007).
[8]A. I. Larkin and Yu. N. Ovchinnikov, Sov. Phys. JETP **41**, 960 (1975).
[9]S. G. Doettinger, R. P. Huebener, R. Gerdemann, A. Kühle, S. Anders, T. G. Träuble, and J. C. Villégier, Phys. Rev. Lett. **73**, 1691 (1994).
[10]B. Kalisky, Y. Wolfus, Y. Yeshurun, G. Koren, and R. P. Huebener, Physica C **401**, 273 (2004).
[11]Z. L. Xiao and P. Ziemann, Phys. Rev. B **53**, 15265 (1996).
[12]Z. L. Xiao and P. Ziemann, Physica C **282–287**, 2363 (1997).
[13]S. L. Ginzburg, A. V. Nakin, and N. E. Savitskaya, Physica C **436**, 7 (2006).
[14]R. J. Wijngaarden, M. S. Welling, C. M. Aegerter, and M. Menghini, Eur. Phys. J. B **50**, 117 (2006).
[15]N. V. Sarlis, P. A. Varotsos, and E. S. Skordas, Phys. Rev. B **73**, 054504 (2006).
[16]F. S. Jelila, J. P. Maneval, F. R. Ladan, F. Chibane, A. Marie-de-Ficquelmont, L. Méchin, J. C. Villégier, M. Aprili, and J. Lesueur, Phys. Rev. Lett. **81**, 1933 (1998).
[17]G. E. Churilov, A. B. Agafanov, D. A. Dikin, and V. M. Dmitriev, Low Temp. Phys. **24**, 555 (1998).
[18]S. Reymond, L. Antognazza, M. Decroux, E. Koller, P. Reinert, and Ø. Fischer, Phys. Rev. B **66**, 014522 (2002).
[19]M. T. Gonzalez, J. Vina, S. R. Curras, J. A. Veira, J. Maza, and F. Vidal, Phys. Rev. B **68**, 054514 (2003).
[20]J. Vina, M. T. Gonzalez, M. Ruibal, S. R. Curras, J. A. Veira, J. Maza, and F. Vidal, Phys. Rev. B **68**, 224506 (2003).
[21]M. Ruibal, G. Ferro, M. R. Osorio, J. Maza, J. A. Veira, and F. Vidal, Phys. Rev. B **75**, 012504 (2007).
[22]R. G. Mints and E. H. Brandt, Phys. Rev. B **54**, 12421 (1996).
[23]D. V. Denisov, A. L. Rakhmanov, D. V. Shantsev, Y. M. Galperin, and T. H. Johansen, Phys. Rev. B **73**, 014512 (2006).
[24]J. Maza, G. Ferro, M. R. Osorio, J. A. Veira, and F. Vidal, Phys. Rev. B **84**, 214530 (2011).
[25]J. Maza, G. Ferro, J. A. Veir, and F. Vidal, Supercond. Sci. Technol. **26**, 105004 (2013).
[26]P. Bernstein, J. F. Hamet, M. T. González, and M. Ruibal Acuña, Physica C **455**, 1 (2007).
[27]S. R. Currás, P. Wagner, M. Ruibal, J. Viña, M. R. Osorio, M. T. González, J. A. Veira, J. Maza, and F. Vidal, Supercond. Sci. Technol. **14**, 748 (2001).
[28]G. J. H. M. Rijnders, G. Koster, D. H. A. Blank, and H. Rogalla, Appl. Phys. Lett. **70**, 1888 (1997).
[29]F. Sirois, J. Coulombe, F. Roy, and B. Dutoit, Supercond. Sci. Technol. **23**, 034018 (2010).
[30]P. Bernstein, C. McLoughlin, Y. Thimont, F. Sirois, and J. Coulombe, J. Appl. Phys. **109**, 033915 (2011).
[31]P. Li, D. Abraimov, A. Xu, and D. Larbalestier, Supercond. Sci. Technol. **25**, 025002 (2012).
[32]N. D. Khatri, G. Majkic, T. Shi, Y. Chen, and V. Selvamanickam, Supercond. Sci. Technol. **26**, 085022 (2013).
[33]E. Zeldov, N. M. Amer, G. Koren, A. Gupta, and M. W. McElfresh, Appl. Phys. Lett. **56**, 680 (1990).
[34]E. H. Brandt and M. Indenbaum, Phys. Rev. B **48**, 12893 (1993).
[35]E. Zeldov, J. R. Clem, M. McElfresh, and M. Darwin, Phys. Rev. B **49**, 9802 (1994).
[36]M. E. Gaevski, A. V. Bobyl, D. V. Shantsev, Y. M. Galperin, T. H. Johansen, M. Baziljevich, H. Bratsberg, and S. F. Karmanenko, Phys. Rev. B **59**, 9655 (1999).
[37]J. Yoo, J. Lee, S. M. Lee, Y.-H. Jung, D. Youm, and S. S. Oh, Supercond. Sci. Technol. **22**, 125019 (2009).
[38]P. Bernstein and J. F. Hamet, J. Appl. Phys. **95**, 2569 (2004).
[39]P. Bernstein, J. F. Hamet, and Y. Thimont, Physica C **468**, 200 (2008).
[40]Th. Schuster, H. Kuhn, E. H. Brandt, M. Indenbom, M. R. Koblischka, and M. Konczykowski, Phys.Rev. B **50**, 16684 (1994).
[41]F. Laviano, D. Botta, R. Gerbaldo, G. Ghigo, L. Gozzelino, L. Gianni, S. Zannella, and E. Mezzetti, Physica C **404**, 220 (2004).
[42]Y. Jung, K. Kwak, W. Lee, J. Rhee, D. Youm, J. Yoo, Y. H. Han, and B. J. Park, Supercond. Sci. Technol. **25**, 065001 (2012).
[43]R. K. Wijngaarden, R. Griessen, J. Fendrich, and W. K. Kwok, Phys. Rev. B **55**, 3268 (1997).
[44]G. Deutscher and K. A. Müller, Phys. Rev. Lett. **59**, 1745 (1987).
[45]G. Deutscher, IBM J. Res. Dev. **33**, 293 (1989).
[46]A. Gurevitch and L. D. Cooley, Phys. Rev. B **50**, 13563 (1994).
[47]E. Mezzetti, R. Gerbaldo, G. Ghigo, L. Gozzelino, B. Minetti, C. Camerlingo, A. Monaco, G. Cuttone, and A. Rovelli, Phys. Rev. B **60**, 7623 (1999).
[48]Y. Zhu, M. Suenaga, J. Tafto, and D. O. Welch, Phys. Rev. B **44**, 2871 (1991).
[49]C. Goupil, F. Warmont, M. Hervieu, J. F. Hamet, and Ch. Simon, Phys. Rev. B **60**, 1418 (1999).
[50]M. Tinkham, *Introduction to Superconductivity*, 2nd ed. (McGraw-Hill, 1996).
[51]S. Berger, D.-G. Crété, J.-P. Contour, K. Bouzehouane, and J. L. Maurice, Phys. Rev. B **63**, 144506 (2001).
[52]T. Yamaguchi, A. Sugimoto, and I. Iguchi, Physica C **357–360**, 1478 (2001).
[53]P. W. Anderson and Y. B. Kim, Rev. Mod. Phys. **36**, 39 (1964).
[54]E. H. Brandt, Phys. Rev. Lett. **69**, 1105 (1992).
[55]E. H. Brandt, Z. Phys. B **80**, 167 (1990).
[56]S. M. Anlage, B. W. Langley, G. Deutscher, J. Halbritter, and M. R. Beasley, Phys. Rev. B **44**, 9764 (1991).
[57]P. Bernstein, J. Appl. Phys. **111**, 103913 (2012).
[58]M. Decroux, L. Antognazza, N. Musolino, E. de Chambrier, S. Reymond, J. M. Triscone, Ø. Fischer, W. Paul, and M. Chen, IEEE Trans. Appl. Supercond. **11**, 2046 (2001).
[59]T. L. Peterson, I. Maartense, and R. Biggers, IEEE Trans. Appl. Supercond. **5**, 1436 (1995).
[60]A. Ishiyama, M. Yanai, T. Morisaki, H. Ueda, Y. Shiohara, T. Izumi, Y. Iijima, and T. Saitoh, IEEE Trans. Appl. Supercond. **15**, 1659 (2005).
[61]R. C. Duckworth, J. W. Lue, D. F. Lee, R. Grabovickic, and M. J. Gouge, IEEE Trans. Appl. Supercond. **13**, 1768 (2003).
[62]J.-F. Hamet, B. Mercey, M. Hervieu, G. Poullain, and B. Raveau, Physica C **198**, 293 (1992).
[63]J.-F. Hamet, B. Mercey, M. Hervieu, and B. Raveau, Physica C **193**, 465 (1992).
[64]J.-F. Hamet, B. Blanc-Guilhon, A. Taffi, B. Mercey, M. Hervieu, and B. Raveau, Physica C **214**, 55 (1993).